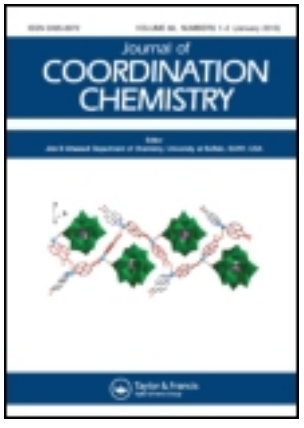

Journal of Coordination Chemistry
Publication details, including instructions for authors and subscription information:
http://www.tandfonline.com/loi/gcoo20

Experimental and quantum chemical studies of sulfamethazine complexes with Ni(II) and Cu(II) ions

A.M. Mansour [a]

[a] Chemistry Department, Faculty of Science , Cairo University , Giza , Egypt

Accepted author version posted online: 14 Feb 2013.Published online: 25 Mar 2013.

To cite this article: A.M. Mansour (2013) Experimental and quantum chemical studies of sulfamethazine complexes with Ni(II) and Cu(II) ions, Journal of Coordination Chemistry, 66:7, 1118-1128, DOI: 10.1080/00958972.2013.775427

To link to this article: http://dx.doi.org/10.1080/00958972.2013.775427

Journal of Coordination Chemistry, 2013
http://dx.doi.org/10.1080/00958972.2013.775427

Experimental and quantum chemical studies of sulfamethazine complexes with Ni(II) and Cu(II) ions

A.M. MANSOUR*

Chemistry Department, Faculty of Science, Cairo University, Giza, Egypt

(*Received 28 May 2012; in final form 10 December 2012*)

$[Ni(SZ)Cl(H_2O)_3]\cdot 2H_2O$ and $[Cu(SZ)(NO_3)(H_2O)_2]\cdot 2H_2O$ (HSZ = 4-amino-*N*-(4,6-dimethyl-2-pyrimidinyl)benzenesulfonamide, sulfamethazine) have been synthesized and characterized by experimental and theoretical methods at the DFT/B3LYP/LANL2DZ level of theory. Ni(II) is coordinated by sulfonamidic (N15) and pyrimidic (N23) of the sulfamethazine drug, three water molecules, and one chloride forming a distorted octahedral geometry, while the Cu(II) complex has a square pyramidal geometry with the same ligand N,N active binding sites. Natural bond orbital (NBO) analysis of CuSZ reveals the participation of the coordinated NO_3^- in triple H-bonds of different strengths with hydrated water molecules, LP(2)O33 $\rightarrow \sigma^*$(O45–H46), LP(2)O40 $\rightarrow \sigma^*$(O45–H44), and LP(2) O38 $\rightarrow \sigma^*$(O48–H47). The voltammogram of NiSZ shows one cathodic and one anodic peak. The complexes and NaSZ were screened for their antibacterial activity.

Keywords: Sulfamethazine; Antimicrobial; LANL2DZ; TD-DFT; Electrochemical

1. Introduction

Many biologically active compounds possess modified pharmacological and toxicological potentials when administered as metal-based compounds [1]. Prominent biological activity of various sulfonamide metal complexes has been reported with antibacterial [2], antitumor, diuretic, anti-carbonic anhydrase [3], hypoglycemic, anti-thyroid, rotease inhibitor, and several other activities [4]. For example, zinc-sulfadiazine has been used to prevent bacterial infection in burned animals [5], while silvadene (2-sulfanilamido-pyrimidine-silver) has been commercially used for treatment of topical burns [6]. Sulfamethazine (4-amino-*N*-(4,6-dimethyl-2-pyrimidinyl) benzene-sulfonamide, HSZ) (Scheme 1) is clinically used in veterinary medicine as an antibacterial compound to treat gastrointestinal and respiratory tract infections [7]. Scheme 1 summarizes the different ligational behavior [8–15] of sulfamethazine toward metal ions. A polymeric CuSZ [14] complex has been synthesized from HSZ, not its sodium salt, in the presence of ammonia solution as a deprotonating agent. Alternatively, 1 : 1 CuSZ and 1 : 2 NiSZ (X = Cl) complexes [11] with pyrimidic and sulfonyl O as ligand active binding sites (Scheme 1, mode II), unlike my findings, were synthesized from HSZ also at pH 8. Various biological aspects [16] of metal complexes exclusively depend on the ease of cleaving the M–L bond. Therefore, it is essential to understand the

*Email: mansour@sci.cu.edu.eg

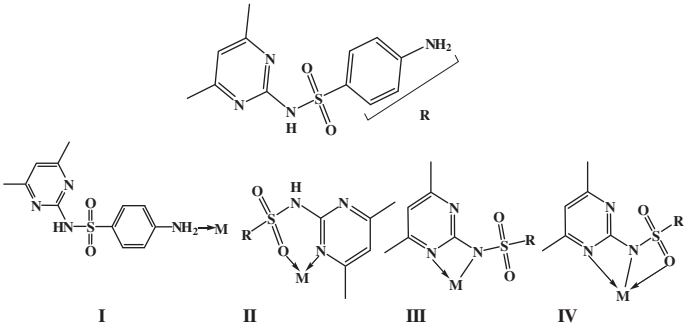

Scheme 1. The reported ligational behavior of sulfamethazine drug.

coordination behavior and relationship of the metals and ligands in biological systems. As continuation of studies [17–19] on biologically active compounds and their coordination compounds and seeking to contribute to the understanding of antibacterial behavior of sulfamethazine upon complex formation, synthesis, characterization, electrochemical, and biological studies on 1 : 1 (M : L) Ni(II) (X = Cl) and Cu(II) ($X = NO_3^-$) sulfamethazine complexes (figure 1) are discussed. To understand the electronic structures of complexes, and the related experimental observations, time-dependent density functional theory (TD-DFT) calculations have also been applied.

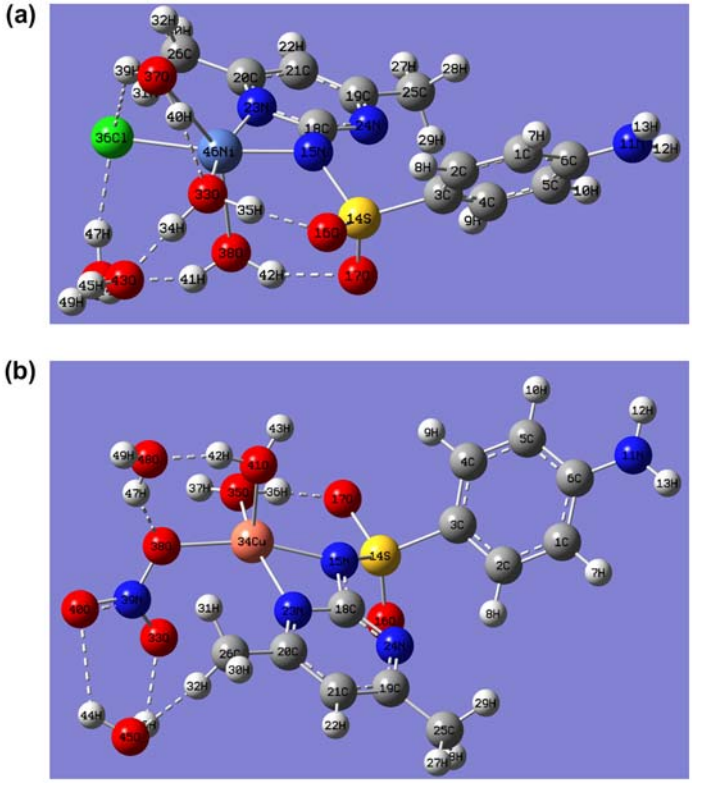

Figure 1. Optimized structures of (a) $[Ni(SZ)(OH_2)_3Cl]\cdot 2H_2O$ and (b) $[Cu(SZ)(NO_3)(H_2O)_2]\cdot 2H_2O$.

2. Experimental

2.1. *Synthesis and characterization*

An aqueous solution of sodium sulfamethazine (NaSZ, 0.301 g, 1 mmol) was added to an aqueous solution of metal ions (1 mmol; $NiCl_2 \cdot 6H_2O$ or $Cu(NO_3)_2 \cdot 3H_2O$) and refluxed for 2 h whereupon the complexes precipitated. Elemental analyzes are in agreement with those calculated for the suggested formulas. The low conductance values of complexes in DMF indicate their non-electrolytic nature.

- Data for NaSZ ($C_{12}H_{13}N_4NaO_2S$). Color: white. Anal. Calcd C, 47.99%; H, 4.36%; N, 18.66. Found: C, 47.80%; H, 4.29%; N, 18.57%. FT IR: 3425, $\nu_{ass}(NH_2)$; 3355, $\nu_{ss}(NH_2)$; 3056, $\nu(CH)_{Ar}$; 1641, $\nu(CN)$; 1569, $\nu(CC)$; 1495, $\delta(NH_2)$; 1422, $\nu(CC)$; 1295, $\nu_{ass}(SO_2)$; 1135, $\nu_{ss}(SO_2)$; 1074, $\rho(NH_2)$; 984, $\nu(SN)$; 677, $\nu(CS)$; and 597 cm^{-1}, $\omega(NH_2)$. UV–vis (DMF): 260, and 274 nm.
- Data for $Ni^{II}SZ$ ($C_{12}H_{23}ClN_4NiO_7S$). Color: pale blue. Anal. Calcd C, 31.23%; H, 5.02%; N, 12.14%; Ni, 12.72. Found: C, 31.10%; H, 4.89%; N, 11.93%; Ni, 12.57%. MS: M^+ 462, $m/z = 445$, 407, 373, 363, 342, 337, 336, 321, 318, 307, 301, 285, 181 and 80. FT IR: 3444, $\nu_{ass}(NH_2)$; 3361, $\nu_{ss}(NH_2)$; 3157, $\nu(CH)_{Ar}$; 1590, $\nu(CC)$; 1557, $\delta(H_2O)$; 1499, $\delta(NH_2)$; 1438, $\nu(CC)$; 1136, $\nu_{ss}(SO_2)$; 1073, $\rho(NH_2)$; 800, $\rho_r(H_2O)$; 672, $\nu(CS)$; and 599 cm^{-1}, $\omega(NH_2)$. UV–vis (DMF): 274, 389, 575, and 660 nm. Molar Cond. (10^{-3} M, DMF): 7.85 $\Omega^{-1}\,cm^2\,mol^{-1}$. $\mu_{eff} = 3.56$ B.M. (296 K).
- Data for $Cu^{II}SZ$ ($C_{12}H_{21}CuN_5O_9S$). Color: Brown. Anal. Calcd C, 30.35%; H, 4.46%; N, 14.75%; Cu, 13.38%. Found: C, 30.18%; H, 4.39%; N, 14.64%; Cu, 13.27%. MS: M^+ 476, $m/z = 460$, 445, 421, 402, 386, 376, 354, 344, 333, 304, 286, 279, 254, 239, 226, 214, 198, and 156. FT IR: 3538, $\nu(OH)_w$; 3454, $\nu_{ass}(NH_2)$; 3360, $\nu_{ss}(NH_2)$; 3142, $\nu(CH)_{Ar}$; 2925, $\nu(CH)_{Aliph}$; 1591, $\nu(CC) + \nu(CN)$; 1557, $\delta(H_2O)$; 1499, $\delta(NH_2)$; 1437, $\nu(CC)$; 1134, $\nu_{sy}(SO_2)$; 1077, $\rho(NH_2)$; 786, $\rho_r(H_2O)$; 740, 730, $\nu_4(NO_3)$; 672, $\nu(CS)$; and 597 cm^{-1}, $\omega(NH_2)$. UV–vis (DMF): 289, 390 and 614 nm. Molar Cond. (10^{-3} M, DMF): 5.35 $\Omega^{-1}\,cm^2\,mol^{-1}$. $\mu_{eff} = 1.90$ B.M. (296 K).

2.2. *Instrumentation*

Infrared spectra were recorded as KBr pellets using FTIR-460 plus, JASCO, while EIMS was monitored with a SHIMADZU QP-2010 plus mass spectrometer at 70 eV. Electronic absorption spectra were obtained using UV–vis SHIMADZU Lambda 4B automated spectrophotometer. X-ray powder diffraction patterns were studied over $2\theta = 5$–$60°$ range using a Philips X-ray diffractometer model PW 1840. Radiation was provided by copper anode (K_α, $\lambda = 1.54056$ Å) operated at 40 kV and 25 mA. TG/DTA analysis was carried out in a dynamic nitrogen atmosphere (20 mL min^{-1}) with a heating rate of 10 °C min^{-1} in a Pt crucible using DTG-60H Simultaneous DTA-TG Apparatus-SHIMADZU. Elemental microanalyses were performed at the Micro-analytical Center, Cairo University. Metal content was determined by complexometry [20]. A digital *Jenway 4310* conductivity-pH meter with (1.02) cell constant was used for molar conductance measurements. Magnetic measurements were carried out on a Sherwood Scientific magnetic balance using the Gouy method [21]. Diamagnetic corrections were made by Pascal's constant and $Hg[Co(SCN)_4]$ was used as a calibrant. Cyclic voltammetry measurements were performed using a

three-electrode configuration cell connected to an EG and G scanning potentiostat model 372 with a scan rate of 100 mV s^{-1}. A Pt disk was used as a working electrode, a Pt wire as an auxiliary electrode and Ag/AgCl electrode as a reference. An amount of 50 ml (10^{-3} M) of sample solution in DMF with 0.1 M $LiClO_4$ as supporting electrolyte was used for the measurements.

2.3. *Computational details*

Density functional theory (DFT) calculations were carried out using the Gaussian 03 package [22]. $[Ni(SZ)Cl(H_2O)_3]\cdot 2H_2O$ was optimized in the ground singlet state using B3LYP/LANL2DZ method [19], while $[Cu(SZ)(NO_3)(H_2O)_2]\cdot 2H_2O$ was optimized in the doublet state using UB3LYP/LANL2DZ. The optimized geometries were verified by performing a frequency calculation at the same level of theory. Vibrational modes were analyzed via Gaussview software [23]. NBO calculations [24] were performed by LANL2DZ basis set providing contribution of atomic orbitals to NBO σ and π hybrid orbitals for bonded atom pairs. Three NBO hybrid orbitals are defined, bonding orbital (BD), lone pair (LP), and core (CR), which were analyzed on the atoms directly bonded to the metal ion (Supplementary material). Frontier molecular orbitals (FMO) [25] and molecular electrostatic potential (MEP) were performed at the same level of theory (Supplementary material).

2.4. *Biological activity*

Antimicrobial activities were carried out using culture of *Bacillus subtilis* and *Staphylococcus aureus* as Gram-positive bacteria and *Escherichia coli* and *Pseudomonas aeruginosa* as Gram-negative bacteria according to a modified Kirby-Bauer disk diffusion method [26] under standard conditions using Mueller-Hinton agar medium (tested for composition and pH), as described by NCCLS [27]. Solution of each compound (20 mg/ml studied compounds and standard drug Tetracycline) in DMSO was prepared for testing against bacteria. Centrifuged pellets of bacteria from a 24 h old culture containing approximately 10^4–10^6 CFU (colony forming units) per ml were spread on the surface of Muller–Hinton agar plates. Then, the wells were seeded with 10 ml of prepared inocula to have 10^6 CFU/ml. Petri plates were prepared by pouring 100 ml of seeded nutrient agar. DMSO (0.1 ml) alone was used as a control under the same conditions for each microorganism.

3. Results and discussion

3.1. *Vibrational assignments*

FTIR spectra of NaSZ and its complexes show numerous bands and assignment of experimental frequencies is not easy. Calculation of the vibrational frequencies aids assignment of the reported spectra. Calculated wavenumbers are higher than the experimental, owing to anharmonicity and basis set deficiencies [28,29]. Scale factors were introduced [30] to overcome these shortcomings. Here, a *uniform* scaling factor of 0.970 is introduced. Experimentally, the primary amino group is not involved in chelation since its stretching modes, $\nu_{ass}(NH_2)$ and $\nu_{ss}(NH_2)$, are located at higher wavenumbers, 3444–3454 and 3360–3366 cm^{-1}, than NaSZ, 3425 and 3355 cm^{-1} [19]. This is confirmed theoretically by existence of these modes in the same position in NaSZ and its complexes, 3661

and 3527 cm^{-1}. The discrepancy [18] between experimental data and DFT calculations may arise from calculations performed in the gaseous state, whereas packing with intermolecular interactions affect experimental measurements. Bands at 1073–1077 and 597–599 cm^{-1} in NaSZ and its complexes are attributed to ρNH_2 (rocking) and ωNH_2 (wagging) modes.

The band at 1641 cm^{-1} in NaSZ is assigned to ν(C=N) mode with some interaction toward sodium ion [21]. This band shifts to lower wavenumbers in complexes and overlaps with ν(C=C) and $\delta(NH_2)$ in the same region. This behavior supports contribution of pyrimidic nitrogen in chelation. The un-scaled ν(C=N) mode is at 1601 cm^{-1} in complexes, where the scaling is not necessary for this type of vibrational mode as already pointed out by Abdel-Ghani *et al*. [17–19]. The $\nu_{ss}(SO_2)$ in complexes is observed at the same position as NaSZ; the $\nu_{ass}(SO_2)$ overlaps with ν(C=C) due to shift of ν(CC) to lower wavenumbers as a result of participation of pyrimidine in chelation. This also may be interpreted in terms of participation of SO_2 in H-bonds with coordinated and hydrated water molecules (discussed later). The position of ν(C-S) remains unaltered in NaSZ and its complexes at 672–674 cm^{-1} excluding coordination of the drug through the sulfonic (SO_2). The ν(S–N) at 984 cm^{-1} in NaSZ compared with 945 cm^{-1} [13] in HSZ indicates interaction between N15 and Na^+ [21]. In complexes, ν(S–N) is at 982 cm^{-1} revealing participation of sulfonamidic N15 in chelation. The nitrato copper complex shows two bands at 740 and 730 cm^{-1} corresponding to $\nu_4(NO_3)$, supporting monodentate nitrate. Experimentally, it is difficult to assign ν_1 and ν_3 of nitrate at 1455–1500 and 1265–1295 cm^{-1} [31], respectively, due to the presence of numerous bands of coordinated sulfamethazine and their coupling with the internal modes of water (bending modes). IR spectrum of NiSZ exhibits a band at 800 cm^{-1} assigned to $\rho_t(H_2O)$; this mode is found at 786 cm^{-1} in CuSZ [18].

Theoretically, NiSZ shows $\nu_{ass}(OH_2)$ of hydrated molecules at 3735 and 3700 cm^{-1}, while the $\nu_{ss}(OH_2)$ mode is located at 3225 and 3141 cm^{-1} for $O43H_2$ and $O48H_2$, respectively. Moreover, the $\nu_{ass}(OH_2)$ for the coordinated water ($O37H_2$, $O38H_2$, and $O33H_2$) is at 3666, 3581, and 3072 cm^{-1}, whereas their symmetric vibrations are at 3489, 3400, and 2664 cm^{-1}, respectively. Experimentally, bands at 3551, 3290, and 3157 cm^{-1} are attributed to $\nu_{ass}(OH_2)$ and $\nu_{ss}(OH_2)$ modes. Calculated bands at 574, 508, 451, and 360 cm^{-1} are assigned to ν(Ni–N23), ν(Ni–O33), ν(Ni–N15), and ν(Ni–Cl), respectively. For CuSZ, bands at 3736, 3728, 3709, and 3686 cm^{-1} are assigned to $\nu_{ass}(OH_2)$, while those at 3538, 3330, 3009, and 2677 cm^{-1} are allocated to symmetric modes. The presence of H-bond between $O35H_2$ and the sulfonyl oxygen (O17) leads to shifting of $\nu_{ass}(35OH_2)$ to a lower wavenumber, 2677 cm^{-1}. The scissoring bending modes of these waters are observed at 1626, 1626, 1593, and 1582 cm^{-1} for $O41H_2$, $O48H_2$, $O45H_2$, and $O35H_2$, respectively. The scaled values at 1358, 1188, 930, 689 and 665 cm^{-1} are attributed to $\nu_1(NO_3)$, $\nu_3(NO_3)$, $\nu_2(NO_3)$, $\nu_4(NO_3)$, and $\nu_5(NO_3)$ of the monodentate nitrate.

3.2. *Mass spectrometry and thermal analysis (TG/DTA)*

The mass spectrum of NiSZ gives M^+ at *m/z* 462 (Supplementary material), assigned to $[Ni(SZ)(OH_2)_3Cl]\cdot 2H_2O$, and its fragmentation pattern is shown in Supplementary material. The presence of two hydrated water molecules in the molecular ion peak may be attributed to H-bonds. The fragments at *m/z* 318, 301, and 285 confirm participation of sulfonamidic nitrogen in chelation.

Three endothermic stages at 62, 434, and 700 °C are observed in TG/DTG curves of NiSZ. One water molecule is lost from ambient to 62 °C, 3.90% (calcd 3.90%). The other hydrated molecule is eliminated at 62–250 °C, revealing presence of stronger interaction [19]. The second degradation step removes $2H_2O$, Cl, SO_2 and aniline with a mass loss of 48.95% (calcd 49.24%). The third step is attributed to removal of remaining organic part with overall mass loss of 83.87% (calcd 83.98%), leaving NiO as residue.

The molecular ion peak of CuSZ is at *m/z* 476 (Supplementary material), assigned to $[Cu(SZ)(NO_3)(H_2O)_2]\cdot 2H_2O$. Fragmentation pattern of this complex goes under three decomposition routes as shown in Supplementary material. The first pathway gives a peak at *m/z* 421, $([Cu(SZ)(NO_3)(H_2O)])^+$. This fragment reveals coordination of NO_3^- as confirmed by conductivity measurements. The second route forms $[Cu(SZ)(H_2O)_2]$, *m/z* 377. The third route gives a fragment at *m/z* 279 due to ligand [30]. The first thermal stage is combined with three endothermic overlapping peaks at 39, 48 and 206 °C, assigned to stepwise desorption of three water molecules with a mass loss of 11.16% (calcd 11.34%). The second and third degradations, maximized at 289 and 386 °C, involve elimination of H_2O, NO, O_2 and one ligand molecule leaving CuO as a residue, 17.21% (calcd 16.70%).

3.3. *Electronic structure, frontier molecular orbitals and magnetic susceptibility*

FMO's play an important role in electric and optical properties [25] and the frontier orbital gap can be used to characterize the chemical reactivity and kinetic stability of the molecule. Supplementary material shows electron distributions and energy levels of HOMO and LUMO orbitals for the reported complexes. The energy gap is 4.59 and 0.12 eV for NiSZ and CuSZ, respectively.

Electronic transitions observed in the UV–vis spectra have been studied by TD-DFT. The lowest 30 spin-allowed excitation states were taken into consideration for calculation of electronic absorption spectra of complexes. The absorption spectra were simulated using GaussSum [32]. Each excited state was interpolated by a Gaussian convolution with the full-width at half-maximum (FWHM) of 3000 cm^{-1}. Table 1 presents the most important electronic transitions and their assignments of the reported complexes. For the high-energy part of the spectrum, only transitions with oscillator strengths ($f > 0.004$) are tabulated. The assignment of calculated orbital excitations to experimental bands was based on an overview of the contour plots and relative energy of occupied and unoccupied molecular orbitals involved in the electronic transitions; d–d transitions are forbidden and their oscillator strengths are very small (close to 0.0).

Sulfanilamide and its sulfonamide N-substituted derivatives exhibit a single absorption at 260 nm [8,9]. Here, the electronic spectrum of NaSZ shows bands at 260 and 274 nm in DMF. The calculated absorption spectrum of CuSZ in the gaseous state (Supplementary material) shows mainly three absorptions at 908, 589, and 388 nm with oscillator strengths 0.003, 0.0068, and 0.0191, respectively. The lowest energy band at 908 nm arises from a transition of β-spin HOMO-1 to β-spin LUMO with total configuration interaction coefficient up to 0.35, while the excitation energy at 589 nm (2.10 eV) is contributed mainly from HOMO(β) → LUMO(β) (63%) transition. These two transitions are typical for square pyramidal copper(II) complexes. The electronic transition at 388 nm (3.19 eV) is assigned to HOMO-6(β) → LUMO(β) (26%). Experimentally, the electronic spectrum of CuSZ exhibits a band at 390 nm assignable to the N(σ) → Cu(II) charge transfer (LMCT) transition along with a band at 289 nm due to $\pi \rightarrow \pi^*$ in the sulfa drug. The band observed at

Table 1. Experimental and computed excitation energies (eV), electronic transition configurations and oscillator strengths (*f*) of the studied complexes.

Exp. λ (nm)		*E* (eV)	*f*	Major contribution	Character
$[Ni(SZ)(OH_2)_2Cl]\cdot 2H_2O$					
	835	1.48	0.0	HOMO-4 → LUMO (73%)	$\pi(SO_2N)/\pi(An)/\pi(NH_2) \rightarrow \pi^*(Py)/d_{Z^2}$
575	609	2.04	0.0015	HOMO-19 → LUMO (25%)	$\pi(H_2O) \rightarrow \pi^*(Py)/d_{Z^2}$
389	374	3.32	0.0055	HOMO-3 → LUMO (75%)	$\pi(py)/\pi(Cl)/\pi(H_2O)/d \rightarrow \pi^*(Py)/d_{Z^2}$
	369	3.35	0.0638	HOMO-1 → LUMO (53%)	$\pi(Cl)/\pi(N15)/d \rightarrow \pi^*(Py)/d_{Z^2}$
	354	3.50	0.0174	HOMO → LUMO + 1 (30%)	$\pi(H_2O)/d \rightarrow \pi^*(An)$
	317	3.99	0.0091	HOMO-2 → LUMO + 1 (76%)	$\pi(Py)/\pi(Cl)/\pi(H_2O)/d \rightarrow \pi^*(An)$
	295	4.20	0.044	HOMO-2 → LUMO + 2 (30%)	$\pi(Py)/\pi(Cl)/\pi(H_2O)/d \rightarrow \pi^*(An)/\pi^*(Py)/\pi^*(Cl)/\pi^*(NH_2)/d_{Z^2}$
	286	4.34	0.026	HOMO-7 → LUMO (22%)	$\pi(SO_2N)/\pi(Cl)/\pi(An)/\pi(N15) \rightarrow \pi^*(Py)/d_{Z^2}$
274	269	4.61	0.0188	HOMO-9 → LUMO (17%)	$\pi(An)/\pi(Py)/\pi(Cl)/\pi(H_2O)/\pi(SO_2N) \rightarrow \pi^*(Py)/d_{Z^2}$
	262	4.73	0.0562	HOMO → LUMO + 4 (34%)	$\pi(H_2O)/d \rightarrow \pi^*(Py)/\pi^*(An)/\pi^*(NH_2)/\pi^*(SO_2N)$
$[Cu(SZ)(NO_3)(H_2O)_2]\cdot 2H_2O$					
	908	1.36	0.003	HOMO-1(β) → LUMO(β) (35%)	$\pi(NO_3^-)/d \rightarrow \pi^*(An)/\pi^*(Py)/d$
	769	1.61	0.0014	HOMO-12(β) → LUMO(β) (20%)	$\pi(NO_3^-)/\pi(SO_2N)/\pi(An)/\pi(H_2O) \rightarrow \pi^*(An)/\pi^*(Py)/d$
614	627	1.97	0.0018	HOMO-29(β) → LUMO(β) (42%)	$(NO_3^-)/\pi(SO_2)/\pi(H_2O) \rightarrow \pi^*(An)/\pi^*(Py)/d$
	589	2.10	0.0068	HOMO(β) → LUMO(β) (63%)	$\pi(Py)/d\ \pi^*(An)/\pi^*(Py)/d$
	554	2.23	0.0101	HOMO-1(β) → LUMO(β) (54%)	$\pi(NO_3^-)/d \rightarrow \pi^*(An)/\pi^*(Py)/d$
	429	2.88	0.0095	HOMO-2(β) → LUMO(β) (83%)	$\pi(An) \rightarrow \pi^*(An)/\pi^*(Py)/d$
	404	3.06	0.0186	HOMO-5(β) → LUMO(β) (26%)	$\pi(Py)/\pi(SO_2N)/\pi(An)/\pi(NH_2) \rightarrow \pi^*(An)/\pi^*(Py)/d$
390	388	3.19	0.0191	HOMO-6(β) → LUMO(β) (26%)	$(NO_3^-)/\pi(N15) \rightarrow \pi^*(An)/\pi^*(Py)/d$
	332	3.72	0.0111	HOMO-10(β) → LUMO(β) (77%)	$\pi(Py)/\pi(SO_2N)/\pi(An)/\pi(H_2O) \rightarrow \pi^*(An)/\pi^*(Py)/d$
289	305	4.06	0.0043	HOMO-15(β) → LUMO(β) (29%)	$\pi(NO_3^-)/\pi(H_2O) \rightarrow \pi^*(An)/\pi^*(Py)/d$

An: Aniline; Py: Pyrimidine.

614 nm is in agreement with the d-d transition for copper(II) in square pyramidal geometry [33]. The observed molar magnetic susceptibility for CuSZ was corrected for diamagnetism and temperature-independent paramagnetism to provide the fully corrected magnetic moment (μ_{eff}) at room temperature (296 K), 1.90 B.M. ($S = 1/2$, $t_{2g}^6 e_g^3$), which is expected for the d^9 system, in the range 1.90–2.20 B.M., excluding metal–metal interactions, supporting a monomeric complex [34].

The two bands in NiSZ at 575 and 660 nm are assigned to $^3A_{2g} \rightarrow {}^3T_{2g}$ (ν_1) and $^3A_{2g} \rightarrow {}^3T_{1g}(^3F)$ (ν_2), respectively, in an octahedral geometry [35,36]. The primary feature of TD-DFT calculated absorption spectrum of NiSZ in gaseous state shows mainly three absorptions at 286, 374, and 609 nm with oscillator strengths 0.026, 0.0055, and 0.0015, respectively. The lowest energy electronic transition at 609 nm (2.04 eV) characterizes

mainly the transition from HOMO-19 to LUMO, while that at 374 nm (3.32 eV) is assigned to HOMO-3 → LUMO (75%). Moreover, the broad absorption (Supplementary material) at 286 nm (4.34 eV) is contributed mainly from HOMO-7 → LUMO (22%) transition. Other excitation energies with their assignments are tabulated in table 1. The effective magnetic moment (μ_{eff}) value of NiSZ was 3.56 B.M. at 296 K with orbital angular momentum contribution (spin-orbital coupling) [36] for octahedral Ni(II) complexes. Generally, experimental values differ from the spin-only ones (2.83 B.M.), usually being somewhat greater, because the orbital motions of the electrons also contribute to the magnetic moment. The theoretical magnitude of spin μ_{eff} (μ_s) for an octahedral nickel complex is 2.83 B.M., whereas orbital contribution (μ_{s+L}) raises this value to 4.47 B.M. [37]. In the present work, the value of μ exceeds μ_s, but is not high as μ_{s+L} [37]. This is because the electric fields of other atoms, ions, and molecules surrounding metal restrict the orbital motion of the electrons so that the orbital angular momentum and hence the orbital moments are partially quenched.

3.4. *X-ray powder diffraction*

Single crystals of the reported complexes could not be obtained since they are amorphous in nature. The X-ray powder diffraction patterns were recorded over $2\theta = 5$–$60°$ to obtain an idea about the lattice dynamics of these compounds. The values of 2θ, interplanar spacing d (Å) and the relative intensities ($I/I°$) are tabulated in Supplementary material. A comparison between the obtained XRD patterns of the complexes (Supplementary material) revealed the pronounced effect of metal type on the crystallinity of these compounds. The identification of the complexes was done by the known method [19]. Such facts suggest that CuSZ is amorphous, while NiSZ is nanocrystalline [19]. There are five strong diffraction peaks in the NiSZ complex at $2\theta = 10.32°$, 11.23°, 22.77°, 23.64°, and 27.38°, and the interstices of the corresponding crystal faces are 8.56, 7.87, 3.90, 3.76, and 3.25 Å, respectively. The interstice 8.56 Å at $2\theta = 10.32°$ is the interlayer spacing of NiSZ.

3.5. *Geometry optimization*

A view of the optimized structure of $[Ni(SZ)Cl(H_2O)_3]\cdot 2H_2O$ with atom numbering is shown in figure 1. Selected bond distances, angles, and charges are listed in Supplementary material. The nickel is distorted octahedral with bidentate sulfamethazine through sulfonamidic [Ni–N15 = 1.931 Å] and pyrimidic [Ni–N23 = 1.958 Å] nitrogens. One water ($O33H_2$) and one chloride are *trans* ligand binding sites. Two axial waters (O43H2 and O44H2) complete the octahedral geometry with bond lengths 3.260 and 2.577 Å, respectively. Sulfonamidic nitrogen (N15, $-0.804e$) bears more negative charge than pyrimidic N (N23, $-0.537e$), giving different Ni–N15 and Ni–N23 bond distances. As shown in figure 1, the hydrated and coordinated waters have several H-bonds with each other leading to distortion in the octahedral geometry. The details of hydrogen bonding are listed in Supplementary material. S14O16 and S14O17 bond distances are equal, since they participate in two H-bonds of nearly the same strength.

The copper is five coordinate with an N2O3 environment (figure 1) with a distorted square pyramid. The axial site is occupied by oxygen of water [Cu–O41 = 2.180 Å], while the basal plane contains two nitrogens of sulfa drug, [Cu–N15 = 2.028 Å] and [Cu–N23 = 2.079 Å], and two oxygens, one from monodentate NO_3^- [Cu–O38 = 2.036 Å]

and the other from water [Cu–O35 = 1.984 Å]. The angular structural index parameter τ [38] expressed here as the difference between bond angles N15–Cu–O38 and N23–Cu–O35 divided by 60 has a value of 0.17. Compared with the ideal values of one for trigonal bipyramid and zero for square pyramid, the τ descriptor of the examined structure indicates squarepyramidal stereochemistry. The Cu–O38(NO_3) bond distance is in agreement with previously reported copper complexes, 2.029 Å, in which the metal is coordinated by a terminal nitrate. O33 of the nitrate group is close to Cu at 2.986 Å. If this distance is short enough to be considered as Cu–O interaction, the coordination polyhedron around Cu is highly distorted octahedral. A summary of H-bond contacts is given in Supplementary material. The coordinated NO_3^- forms three H-bonds of different strengths with hydrated water, O45H44···O40, O45H46···O33, and O48H47···O38 with distances 2.411, 2.155, and 1.762 Å, respectively. The strongest H-bond of nitrate is O48H47···O38 since the angle of interaction is 144.5° [19]. As shown in figure 1, one hydrated water ($O48H_2$) bridges between the axial water molecule and NO_3^- through two H-bonds, O41H42···O48 and O48H47···O38.

3.6. *Electrochemical studies*

NaSZ is oxidized in one irreversible one-electron process at $E_{1/2}$ 0.69 V (Supplementary material) characteristic of *p*-amino group [39], leading to azo-hydrazo species as a final product. The oxidation process is associated with a cathodic peak at −1.10 V due to reduction in sulfonamide group. On scanning from 0.0 to −1.5 V, the voltammogram of $[Ni(SZ)Cl(OH_2)_3]\cdot 2H_2O$ shows one well separated peak in the cathodic scan at −0.77 V corresponding to reduction in Ni(II)–Ni(I) [40] and one anodic peak at −1.04 V, assigned to oxidation of Ni(II)–Ni(III) [41]. The voltammogram of CuSZ shows one cathodic peak at −0.92 V which may be attributed to reduction in metal center [42], while the oxidation of Cu(II)/Cu(III) occurs at −1.06 V. The observed E^o value indicates considerable hard acid character due to participation of pyrimidic and sulfonamidic nitrogens in chelation.

3.7. *Antimicrobial activity*

Sodium sulfamethazine and its complexes were screened *in vitro* for their antibacterial activity against *B. subtilis* and *S. aureus* as Gram-positive bacteria and *E. coli* and *P. aeruginosa* as Gram-negative bacteria by a modified Kirby-Bauer disk diffusion method [26]. As shown in Supplementary material, sodium sulfamethazine has the capacity of inhibiting the metabolic growth of the investigated bacteria to different extents and is slightly more efficient than tetracycline. The complexes have ability to kill the investigated bacteria with large inhibition zone diameters comparing with that of NaSZ, but at higher concentration than the sodium salt.

Sulfonamides penetrate bacterial cells in the neutral form, and once inside a cell, their bacterial action is from the ionized form [43]. For CuSZ complex, the activity was slightly higher than the free ligand, but NiSZ less.

4. Conclusion

Synthesis of Ni(II) and Cu(II) complexes coordinated by sulfamethazine drug from sulfamethazine sodium salt, not its free acid, in the absence of a deprotonating agent has been developed. Sulfamethazine is a mono-negative bidentate ligand, interacting with metal through pyrimidic and sulfonamidic nitrogens. The reasonable agreement between theoretical and experimental data reflects the suitability of the applied basis set, LANL2DZ, for this type of work and confirms the suggested structures. NBO analysis shows that the 3d-electron population of 8.65 does not correspond to Ni(II), in agreement with ligand to d_{Ni} electron transfer. The σ(S14–O16) and σ(S14–O17) form from nearly the same $sp^{3.11}$ hybrid on sulfur (75.65% p) and leads to consistency in the SO_2 bond distance. MEP analysis reveals that the most positive region in copper sulfamethazine complex is located over the metal center at the base of the square pyramid, while the amino group in nickel complex is the most active nucleophilic attack site. The strength of the M–L bonds affects the biological activity.

References

[1] A.R. Timerbaev, C.G. Hartinger, S.S. Aleksenko, B.K. Keppler. *Chem. Rev.*, **106**, 2224 (2006).
[2] T.H. Maren. *Annu. Rev. Pharmacol. Toxicol.*, **16**, 309 (1976).
[3] C.T. Supuran. *Nat. Rev. Drug Discovery*, **7**, 168 (2008).
[4] M. Ruiz, L. Perello, R. Ortiz, A. Castineiras, C. Maichlemossmer, E. Canton. *J. Inorg. Biochem.*, **59**, 801 (1995).
[5] (a) N.C. Baenziger, S.L. Modak, C.L. Fox. *Acta Crystallogr.*, **C39**, 1620 (1983). (b) C.J. Brown, D.S. Cook, L. Sengier. *Acta Crystallogr.*, **C41**, 718 (1985).
[6] (a) N.C. Baenziger, A.W. Struss. *Inorg. Chem.*, **15**, 1807 (1976). (b) D.S. Cook, M.F. Turner. *J. Chem. Soc., Perkin Trans. 2*, 1021 (1975).
[7] F. de Zayas-Blanco, M.S. García-Falcón, J. Simal-Gándara. *Food Control*, **15**, 375 (2004).
[8] K.K. Narang, J.K. Gupta. *Transition Met. Chem.*, **2**, 83 (1977).
[9] K.K. Narang, J.K. Gupta. *Transition Met. Chem.*, **2**, 181 (1977).
[10] M.K. Hassan, R.M. Hassan, M.A. Abd-Alla. *Monatsh. Chem.*, **122**, 829 (1991).
[11] W.M. Hosny. *Synth. React. Inorg. Met-Org. Chem.*, **27**, 197 (1997).
[12] L. Gutiérrez, G. Alzuet, J. Borrás, A. Castiñeiras, A. Rodríguez-Fortea, E. Ruiz. *Inorg. Chem.*, **40**, 3089 (2001).
[13] G.M. Golzar Hossain, A.J. Amoroso, A. Banu, K.M.A. Malik. *Polyhedron*, **26**, 967 (2007).
[14] J.B. Tommasino, F.N.R. Renaud, D. Luneau, G. Pilet. *Polyhedron*, **30**, 1663 (2011).
[15] A. García-Raso, J.J. Fiol, S. Rigo, A. López-López, E. Molins, E. Espinosa, E. Borrás, G. Alzuet, J. Borrás, A. Castiñeiras. *Polyhedron*, **19**, 991 (2000).
[16] R. X.Yuan, R.G. Xiong, Z.F. Chen, P. Zhang, H.X. Ju, Z. Dai, Z.J. Guo, H.K. Fun, X.Z. You. *J. Chem. Soc., Dalton Trans*., 774 (2001).
[17] N.T. Abdel-Ghani, A.M. Mansour. *Inorg. Chim. Acta*, **373**, 249 (2011).
[18] N.T. Abdel-Ghani, A.M. Mansour. *Eur. J. Med. Chem.*, **47**, 399 (2012).
[19] N.T. Abdel-Ghani, A.M. Mansour. *J. Coord. Chem.*, **65**, 763 (2012).
[20] A. Skoog, D.M. West. *Fundamentals of Analytical Chemistry*, Thomson, Brooks, Cole, New York (2004).
[21] A.M. Mansour. *J. Mol. Struct.*, **1035**, 114 (2013).
[22] M.J. Frisch, G.W. Trucks, H.B. Schlegel, G.E. Scuseria, M.A. Robb, J.R. Cheeseman, V.G. Zakrzewski, J.A. Montgomery, R.E. Stratmann, J.C. Burant, S. Dapprich, J.M. Millam, A.D. Daniels, K.N. Kudin, M.C. Strain, O. Farkas, J. Tomasi, V. Barone, M. Cossi, R. Cammi, B. Mennucci, C. Pomelli, C. Adamo, S. Clifford, J. Ochterski, G.A. Petersson, P.Y. Ayala, Q. Cui, K. Morokuma, D.K. Malick, A.D. Rabuck, K. Raghavachari, J.B. Foresman, J. Cioslowski, J.V. Ortiz, A.G. Baboul, B.B. Stefanov, G. Liu, A. Liashenko, P. Piskorz, I. Komaromi, R. Gomperts, R.L. Martin, D.J. Fox, T. Keith, M.A. Al-Laham, C.Y. Peng, A. Nanayakkara, C. Gonzalez, M. Challacombe, P.M.W. Gill, B.G. Johnson, W. Chen, M.W. Wong, J.L. Andres, M. Head-Gordon, E.S. Replogle, J.A. Pople, *GAUSSIAN 03 (Revision A.9)*, Gaussian, Inc., Pittsburgh (2003).
[23] A. Frisch, A.B. Nielson, A.J. Holder. *GAUSSVIEW User Manual*, Gaussian Inc., Pittsburgh, PA (2000).
[24] F. Weinhold, J.E. Carpenter. *The Structure of Small Molecules and Ions*. p. 227, Plenum, New York, NY (1988).

[25] I. Fleming. *Frontier Orbitals and Organic Chemical Reactions*, Wiley, London (1976).
[26] (a) D. Greenwood. *Antimicrobial Chemotherapy*, Bailliere, Tindall, London. Part II. *Laboratory Aspects of Antimicrobial Therapy* (1983), p. 71; (b) V. Lorian. *Antibiotics in Laboratory Medicine,* Williams & Wilkins, Baltimore (1996).
[27] National Committee for Clinical Laboratory Standards, NCCLS Approval Standard Document M2-A7, Vilanova, PA (2000).
[28] N.T. Abdel-Ghani, A.M. Mansour. *Spectrochim. Acta, Part A*, **81**, 754 (2011).
[29] N.T. Abdel-Ghani, A.M. Mansour. *Spectrochim. Acta, Part A*, **81**, 529 (2011).
[30] N.T. Abdel-Ghani, A.M. Mansour. *J. Mol. Struct.*, **991**, 108 (2011).
[31] A.S. Potapov, A.I. Khlebnikov. *Polyhedron*, **25**, 2683 (2006).
[32] N.M. O'Boyle, A.L. Tenderholt, K.M. Langner. *J. Comput. Chem.*, **29**, 839 (2008).
[33] S. Dey, S. Sarkar, H. Paul, E. Zangrando, P. Chattopadhyay. *Polyhedron*, **29**, 1583 (2010).
[34] G. Albertin, E. Bordignon, A.A. Orio. *Inorg. Chem.*, **14**, 1411 (1975).
[35] E. González, A. Rodrigue-Witchel, C. Reber. *Coord. Chem. Rev.*, **251**, 351 (2007).
[36] S. Chandra, U. Kumar. *Spectrochim. Acta, Part A*, **61**, 219 (2005).
[37] A. Cotton, G. Wilkinson. *Advanced Inorganic Chemistry*, 2nd Edn, John Wiley and Sons, Inc., New York, London, Sydney and Toronto (1972).
[38] J. Pons, A. Chadghan, J. Casabo, A. Alvarez-Larena, J.F. Piniella, J. Ros. *Polyhedron*, **20**, 2531 (2001).
[39] J. Tommasino, F.N.R. Renaud, D. Luneau, G. Pilet. *Polyhedron*, **30**, 1663 (2011).
[40] R.N. Patel, N. Singh, V.L.N. Gundla. *Polyhedron*, **26**, 757 (2007).
[41] M. Mondelli, V. Brune, G. Borthagaray, J. Ellena, O.R. Nascimento, C.Q. Leite, A.A. Batista, M.H. Torre. *J. Inorg. Biochem.*, **102**, 285 (2008).
[42] S. Zolezzi, E. Spodine, A. Decinti. *Polyhedron*, **21**, 55 (2002).
[43] W.O. Foye, T.L. Lemke, D.A. Williams. *Principles of Medicinal Chemistry*, 4th Edn, pp. 709–713, Williams & Williams (1995).